

Emergent microtubule properties in a model of filament turnover and nucleation

Anna C Nelson^{*1}, Scott A McKinley², Melissa M Rolls³, and Maria-Veronica Ciocanel^{4,5}

¹Department of Mathematics & Statistics, University of New Mexico, Albuquerque, NM, 87131, USA

²Department of Mathematics, Tulane University, New Orleans, LA, 70118, USA

³Department of Biochemistry and Molecular Biology, Pennsylvania State University, University Park, PA, 16802, USA

⁴Department of Mathematics, Duke University, Durham, NC, 27710, USA

⁵Department of Biology, Duke University, Durham, NC, 27710, USA

April 17, 2025

Abstract

Microtubules (MTs) are dynamic protein filaments essential for intracellular organization and transport, particularly in long-lived cells such as neurons. The plus and minus ends of neuronal MTs switch between growth and shrinking phases, and the nucleation of new filaments is believed to be regulated in both healthy and injury conditions. We propose stochastic and deterministic mathematical models to investigate the impact of filament nucleation and length-regulation mechanisms on emergent properties such as MT lengths and numbers in living cells. We expand our stochastic continuous-time Markov chain model of filament dynamics to incorporate MT nucleation and capture realistic stochastic fluctuations in MT numbers and tubulin availability. We also propose a simplified partial differential equation (PDE) model, which allows for tractable analytical investigation into steady-state MT distributions under different nucleation and length-regulating mechanisms. We find that the stochastic and PDE modeling approaches show good agreement in predicted MT length distributions, and that both MT nucleation and the catastrophe of large-length MTs regulate MT length distributions. In both frameworks, multiple mechanistic combinations achieve the same average MT length. The models proposed can predict parameter regimes where the system is scarce in tubulin, the building block of MTs, and suggest that low filament nucleation regimes are characterized by high variation in MT lengths, while high nucleation regimes drive high variation in MT numbers. These mathematical frameworks have the potential to improve our understanding of MT regulation in both healthy and injured neurons.

Keywords: microtubule turnover, stochastic modeling, nucleation

^{*}annanelson@unm.edu

1 Introduction

Microtubules (MTs) are important filament structures within cells that are composed of tubulin dimers and are responsible for intracellular organization and transport. In long-lived and long-range cells like neurons, the MT cytoskeleton is required for sustained transport across large spatial and temporal scales [1, 2]. Microtubules are polarized structures with plus and minus ends, and molecular motor proteins are known to carry protein cargo in specified directions along these filaments. Stable MT structures with specific orientations of their plus and minus ends are critical for sorting and continuous transport of proteins to targeted subcellular destinations. However, the MT cytoskeleton remain dynamic throughout the lifetime of the cell. The lengths of individual MTs grow through a process known as dynamic instability, where both the plus and the minus ends stochastically switch between periods of growth and shrinking [3]. Microtubule end dynamics thus regulate the filament length distribution, where MT growth depends on available tubulin dimers, and other microtubule-associated proteins can induce the switch from growth to shrinking, called catastrophe [2]. New MTs are nucleated and regulated by γ -tubulin ring complexes, which act as a template [4]. Microtubule nucleation is believed to be tightly controlled throughout the lifetime of living neurons [5, 6, 7, 8].

Due to the complex nature of MT dynamics, mathematical models have long been used to describe MT behavior and give insights into important biological mechanisms. For example, studies of the search-and-capture models of MTs and chromosome interactions use mean-field partial differential equation (PDE) models and focus on understanding MT search times in mitosis and cell division [9, 10]. Many other studies also use PDEs to describe the process of dynamic instability of MTs at their plus end, sometimes incorporating finer details such as GTP hydrolysis mechanisms [11, 12, 13, 14, 15]. Some models also account for MT length regulation mechanisms, such as limited tubulin availability [16, 17, 18, 19, 20, 21] or various length- or age-dependent regulation of MT growth and shrinking [22, 23, 24, 25, 26, 15, 27]. Fewer studies consider the impact of nucleation on MT length dynamics: in [19, 28], the authors used PDE models to incorporate tubulin-dependent nucleation and growth of MTs, while the authors in [29, 30] used stochastic modeling to show that changes in nucleation can impact plus-end MT dynamics and filament lengths. However, understanding emerging MT lengths and numbers in complex cell environments requires a rigorous characterization of how multiple mechanisms contribute to these filament properties. In particular, we expect that nucleation, growth and shrinking at both MT ends, and MT length-regulation mechanisms all impact the behavior of non-centrosomal MTs in neuronal cells.

While MT dynamics have been studied extensively *in vitro*, here we are interested in understanding MT dynamics and regulation in living neurons. In a previous study, we used stochastic modeling to understand how different length-regulation mechanisms can impact key MT quantities such as MT growth speeds and length distributions [21]. In that study, we were motivated by the experimental evidence that tubulin in MTs turns over every few hours [31]. By analyzing a representative mean-field differential equation model

of MT turnover, we parameterized the stochastic model in order to capture realistic *in vivo* behavior. In particular, simulations of this model matched observed distributions of speeds at both MT ends and predicted that MT length control and distributions depend on the mechanisms contributing to length regulation.

Our prior work [21] assumed a fixed number of MTs, driven by the observation that nucleation is heavily regulated in neurons [32, 33]. However, *in vivo* experiments also suggest that nucleation is up-regulated during neuronal injury [34, 32, 35, 36] and that injury induces a global increase in MT dynamics in both fruit fly and mammalian neurons [32, 37]. Even in healthy neurons, nucleation can also increase at presynaptic sites by up-stream neuronal activity [38]. However, it is not well understood or characterized how various MT growth mechanisms interact with MT nucleation to impact attributes such as the number of MTs and the MT length distributions. Here, we use our model of MT turnover with length-regulating mechanisms at both ends [21] to study the impact of nucleation on stochastic fluctuations in both tubulin availability and in the MT numbers. We further develop a reduced PDE model that describes the MT dynamics at the plus ends of MTs and allows for variation in MT numbers to analytically determine the relationship between tubulin allocation and average MT lengths and numbers. We show that steady-state analysis of the PDE model provides good agreement with stochastic model results, and that the stochastic model is needed to predict the spread in MT length and number in different nucleation and length-regulation regimes.

2 Stochastic model of microtubule growth and nucleation

To understand how MT nucleation affects MT numbers and turnover dynamics, we first adapt the stochastic CTMC (continuous-time Markov chain) model of microtubule dynamics we originally developed in [21]. Figure 1(a) shows an outline of this CTMC model framework with nucleation, where the previously-published MT turnover model mechanisms are shown boxed. Our prior MT turnover model assumes a one-dimensional spatial domain that represents a neuronal dendrite segment with uniform polarity. Each MT is described by the pair $(x_+(t), x_-(t))$, where $x_-(t)$ and $x_+(t)$ refer to the position of the minus and plus end, respectively. For all times t , we assume $x_+(t) \geq x_-(t)$. MT ends can be in one of two states: shrinking, where the MT is depolymerizing, or growth, where the MT end is polymerizing. Microtubule ends switch from shrinking to growth at the plus end with rate $\lambda_{s \rightarrow g}^+$ and from growth to shrinking at the plus end with rate $\lambda_{g \rightarrow s}^+$. In the shrinking state, the MT plus ends shrink with velocity v_s^+ , and in the growth state, the plus ends grow with velocity v_g^+ . Similar notation is used to describe the dynamics at the MT minus ends.

Here, we model MT nucleation as a Poisson process with rate ν , so that in one time step Δt , the probability of nucleating k microtubules is given by

$$P(k \text{ nucleated MTs in time step } \Delta t) = \frac{(\nu \Delta t)^k e^{-\nu \Delta t}}{k!}. \quad (1)$$

Each nucleated microtubule is seeded at length 0 and we assume that both MT ends start

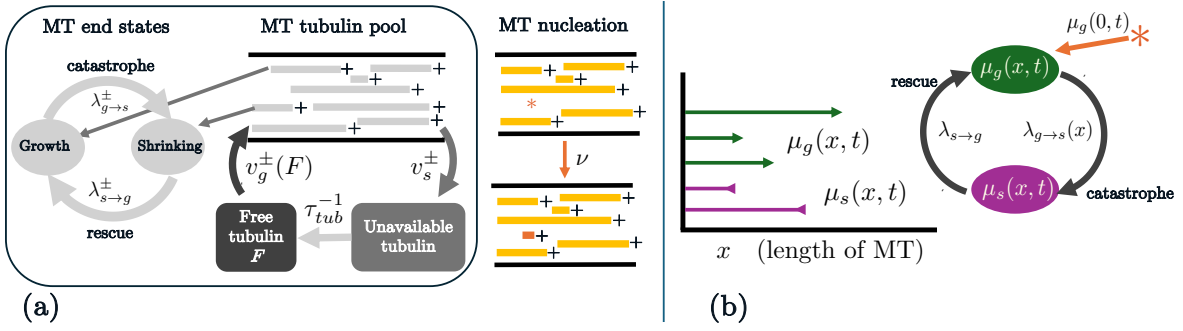


Figure 1: (a) Schematic of the CTMC model of MT growth/shrinking dynamics and nucleation. The boxed portion of the schematic was previously developed in [21]. (b) Schematic of the PDE model of MT growth dynamics at the plus end, where nucleation of MTs occurs only for the growing MT population of length 0, i.e. $\mu_g(0, t)$.

in growth phase at nucleation.

In our original model of MT polymerization dynamics, we aimed to understand how two mechanisms—tubulin-dependent growth and length-dependent catastrophe—contribute to regulating MT length. These length regulation mechanisms are also relevant for the setting here, where the number of MTs is variable. Figure 1(a) illustrates how the two mechanisms are incorporated into our stochastic simulation: the MT growth velocity is assumed to depend on the availability of free tubulin, while the switching rate from growth to shrinking is a function of the length of the microtubule. Tubulin protein is assumed to be either in microtubules ($M(t)$) or available throughout the cell for growth ($F(t)$). Microtubule growth is therefore regulated by the amount of free tubulin, while shrinking events release tubulin and lead to an increase in $F(t)$. Throughout the simulation, we assume that the amount of tubulin in the cell is fixed, so that $T_{tot} = M(t) + F(t)$. For tubulin-dependent growth, we model the growth velocity using a Michaelis-Menten mechanism in order to capture the saturating effect of tubulin. The growth velocity on either the plus or minus end of each MT is therefore given by

$$\begin{aligned} v_g^\pm(F(t)) &= v_g^{\pm, max} \frac{F(t)}{F_{1/2} + F(t)} \\ &= v_g^{\pm, max} \frac{T_{tot} - M(t)}{F_{1/2} + T_{tot} - M(t)}. \end{aligned} \quad (2)$$

For the length-dependent catastrophe mechanism, we assume that the switching rate from growth to shrinking on either MT end varies linearly with the MT length x :

$$\lambda_{g \rightarrow s}(x) = \max \left(\lambda_{\min}, \lambda_{g \rightarrow s}^0 + \gamma(x - L_0) \right). \quad (3)$$

Here, $\lambda_{g \rightarrow s}^0$ is the experimental growth to shrinking switch rate and λ_{\min} is a minimum switch rate that ensures this rate stays positive. For this study, we choose $\lambda_{\min} = 0.1 \text{ min}^{-1}$, so that $\lambda_{\min} < \lambda_{g \rightarrow s}^0$. L_0 is the characteristic MT length; if $x = L_0$, the growth to catastrophe switching rate is equal to the experimental switching rate, $\lambda_{g \rightarrow s}^0$. Given the expression in

Experimentally-informed quantities	Notation	Plus-end	Minus-end
Max growth-phase speed	v_g^{\max}	9 $\mu\text{m}/\text{min}$ [39]	1.125 $\mu\text{m}/\text{min}$ [39]
Average growth-phase speed	\bar{v}_g	6 $\mu\text{m}/\text{min}$ [39]	0.75 $\mu\text{m}/\text{min}$ [39]
Average growth to shrinking switch	$\lambda_{g \rightarrow s}^0$	0.5 min^{-1} [39]	0.25 min^{-1} [39]
Average growth phase duration	$\bar{\tau}_g$	2 min [39]	4 min [39]
Shrinking-phase speed ($ \text{MT} > 0$)	\bar{v}_s	6 $\mu\text{m}/\text{min}$ ‡	3.5 $\mu\text{m}/\text{min}$ ‡
Prescribed model parameters	Notation	Value(s)	
Total available tubulin	T_{tot}	700 to 4000 μm	
MT nucleation rate	ν	0.01 – 10 min^{-1}	
Number of MT sharing tubulin pool	N	parameterized for 20, varies	
Average MT length	\bar{L}	35 μm	
Characteristic MT length	L_0	35 μm	
Length-dependence of catastrophe rate	γ	0 to 0.03 ($\mu\text{m} \cdot \text{min}$) $^{-1}$	
Minimum growth to shrinking switch rate	λ_{\min}	0.1 min^{-1}	
Polymerization/depolymerization speeds	v_g, v_s	v_g^{\max}, \bar{v}_s	
Catastrophe rates at length L_0	$\lambda_{g \rightarrow s}$	$1/\bar{\tau}_g$	
Michaelis-Menten constant (scarce tubulin)	$F_{1/2}$	parameterized from [21]	
Rescue rates	$\lambda_{s \rightarrow g}$	parameterized from [21]	

Table 1: Model parameters and experimentally-observed quantities that inform parameter choices. Parameters marked with ‡ are preliminary estimates from the Rolls Lab. A full description of the parameterization strategy is addressed in [21].

equation (3), the switching rate from growth to catastrophe will exceed λ_{\min} for all x if $\gamma < (\lambda_{g \rightarrow s}^0 - \lambda_{\min})/L_0 = \gamma_{\text{crit}}$. Otherwise, the minimum rate λ_{\min} will be imposed for short MTs. For further details on these mechanisms, see [21].

2.1 Parameterization for the stochastic model

For the MT turnover model, we use the parameterization procedure outlined in [21], which allows us to tune parameters in the stochastic model so as to obtain outputs that match experimental or estimated measurements of microtubule dynamics at steady state. Table 1 outlines the experimentally-informed quantities and the prescribed model parameters. Several model parameters are chosen to satisfy certain constraints, which are met using a steady-state analysis of a reduced ODE model in [21]. For example, we expect our model to achieve a steady-state MT length, \bar{L} , which is equal to a target experimental MT length, L_* . For more details on the parameterization procedure and the stochastic simulation, we refer to [21].

In the stochastic MT dynamics and nucleation model that we study here, we investigate the key factors that limit microtubule length (resource/tubulin constraints and length-dependent catastrophe), as well as their interaction with the nucleation mechanism and the variable number of MTs. Since a healthy cell could be thought to be at homeostatic equilibrium, we are primarily interested in understanding microtubule behavior at steady state. The stochastic framework can capture fluctuations in behavior both within individual

microtubule trajectories and across multiple trajectories. However, this approach requires a high-dimensional parameter space, the exploration of which is computationally intensive and challenging. To overcome these limitations, in section 3 we propose a coarse-grained deterministic model, formulated using partial differential equations (PDEs), that captures the dynamics at one end of the microtubule.

3 Reduced PDE model of microtubule turnover and nucleation

In the following, we describe a reduced continuous model that allows for more tractable investigation of MT nucleation and of its interaction with the same mechanisms of length regulation as in the stochastic model described in Section 2. This reduced modeling framework for MT dynamics consists of PDEs that track densities of growing and shrinking MTs as a function of MT length and time. These densities provide insights into the distributions of MTs lengths over time or at steady state.

For simplicity, we model MT growth and shrinking at the plus end only in the continuous PDE model framework. Microtubule length x is defined in the semi-infinite domain $x \in [0, \infty)$. Let $\mu_g(x, t)$ and $\mu_s(x, t)$ correspond to densities of growing and shrinking MTs of length x at time t . Then $\mu(x, t) = \mu_g(x, t) + \mu_s(x, t)$ is the size-frequency function that represents the density of MTs with length x at time t . The amount of tubulin in MTs at time t is given by:

$$M(t) = \int_0^\infty x \mu(x, t) dx, \quad (4)$$

and $T(t) = T_{tot} - M(t)$ is the amount of free tubulin. Similarly, the number of MTs at time t is

$$N(t) = \int_0^\infty \mu(x, t) dx. \quad (5)$$

Polymerizing MTs grow with velocity v_g , which depends on the amount of available tubulin $T(t)$. To model the potential scarcity of available tubulin, we use a Michaelis-Menten formulation so that:

$$\begin{aligned} v_g(T(t)) &= v_g^{max} \frac{T(t)}{F_{1/2} + T(t)} = v_g^{max} \frac{T_{tot} - M(t)}{F_{1/2} + T_{tot} - M(t)} \\ &= v_g^{max} \frac{T_{tot} - \int_0^\infty x \mu(x, t) dx}{F_{1/2} + T_{tot} - \int_0^\infty x \mu(x, t) dx}. \end{aligned} \quad (6)$$

Thus the MT growth velocity is also a function of the amount of tubulin in microtubules, i.e. $v_g(M(t))$.

Both plus and minus ends of MTs undergo periods of growth and shrinkage, with switching between these states. As in section 2, we model this through switching rates between the growth and shrinking states. The rate of switching from shrinking to growing is constant, while the rate of switching from growth to shrinking depends on the MT length x , as defined in Equation (3) for the stochastic model.

Together, these mechanisms yield the following time-evolution equations for $\mu_g(x, t)$ and $\mu_s(x, t)$:

$$\begin{aligned}\frac{\partial}{\partial t}\mu_g &= -\frac{\partial}{\partial x}(v_g(M(t))\mu_g) - \lambda_{g \rightarrow s}(x)\mu_g + \lambda_{s \rightarrow g}\mu_s, \\ \frac{\partial}{\partial t}\mu_s &= \frac{\partial}{\partial x}(v_s\mu_s) + \lambda_{g \rightarrow s}(x)\mu_g - \lambda_{s \rightarrow g}\mu_s.\end{aligned}\tag{7}$$

The boundary condition for Eqs. (7) is given by:

$$v_g(M(t))\mu_g(0, t) = \nu,\tag{8}$$

which specifies that the rate of nucleation of MTs of length 0 occurs at rate ν . This is similar to the “sticky” boundary conditions for a model of MT catastrophe in a finite domain considered in [10, 40].

With the established notation, and in analogy with equation (5), we can also define the number of growing and shrinking MTs as

$$N_g(t) = \int_0^\infty \mu_g(x, t)dx, \quad N_s(t) = \int_0^\infty \mu_s(x, t)dx,\tag{9}$$

respectively. Then $N(t) = N_g(t) + N_s(t)$ corresponds to the total number of MTs. Similarly, in analogy with equation (4), the amount of tubulin in growing and shrinking MTs is defined to be

$$M_g(t) = \int_0^\infty x\mu_g(x, t)dx, \quad M_s(t) = \int_0^\infty x\mu_s(x, t)dx,\tag{10}$$

respectively.

3.1 Steady-state analysis of PDE model

As with the stochastic model in Section 2.1, we aim to understand how different mechanisms of MT dynamics influence the steady-state solutions of Eqs. (7). Namely, we wish to solve for $\bar{\mu}_g(x) = \lim_{t \rightarrow \infty} \mu_g(x, t)$ and $\bar{\mu}_s(x) = \lim_{t \rightarrow \infty} \mu_s(x, t)$, which we refer to as the steady-state MT length distribution of growing and shrinking MTs, respectively. We note that this is not a MT length size probability distribution because it does not integrate to one. Rather, these are frequency distributions and for the sake of efficiency we will not emphasize the word frequency. Then

$$\frac{\partial}{\partial t}\bar{\mu}_g = 0, \quad \frac{\partial}{\partial t}\bar{\mu}_s = 0,\tag{11}$$

so that $\frac{\partial}{\partial t}\bar{\mu} = 0$ and

$$\frac{\partial}{\partial t}M(t) = \int_0^\infty x \frac{\partial \bar{\mu}}{\partial t} dx = 0.\tag{12}$$

Therefore, the amount of tubulin in MTs is $M(t) \equiv \bar{M}$ and similarly $\bar{T} \equiv T_{tot} - \bar{M}$. Given Eq. (6), the growth speed at steady state can be written as:

$$\begin{aligned} v_g(\bar{M}) &= v_g^{max} \frac{T_{tot} - \bar{M}}{F_{1/2} + T_{tot} - \bar{M}} \\ &= v_g^{max} \frac{T_{tot} - \int_0^\infty x(\bar{\mu}_g(x) + \bar{\mu}_s(x))dx}{F_{1/2} + T_{tot} - \int_0^\infty x(\bar{\mu}_g(x) + \bar{\mu}_s(x))dx}. \end{aligned} \quad (13)$$

To find the steady-state solutions $\bar{\mu}_g$ and $\bar{\mu}_s$, we solve:

$$\begin{aligned} \frac{\partial}{\partial x} (v_g(\bar{M})\bar{\mu}_g) &= -\lambda_{g \rightarrow s}(x)\bar{\mu}_g + \lambda_{s \rightarrow g}\bar{\mu}_s, \\ \frac{\partial}{\partial x} (v_s\bar{\mu}_s) &= -\lambda_{g \rightarrow s}(x)\bar{\mu}_g + \lambda_{s \rightarrow g}\bar{\mu}_s. \end{aligned} \quad (14)$$

Subtracting Eqs. (14) yields

$$\frac{\partial}{\partial x} (v_g(\bar{M})\bar{\mu}_g(x) - v_s\bar{\mu}_s(x)) = 0, \quad (15)$$

which can be integrated to obtain

$$v_g(\bar{M})\bar{\mu}_g(x) - v_s\bar{\mu}_s(x) = C_1. \quad (16)$$

Microtubule lengths are bounded, therefore we set

$$\lim_{x \rightarrow \infty} \bar{\mu}_g(x) = \lim_{x \rightarrow \infty} \bar{\mu}_s(x) = 0, \quad (17)$$

which implies that $C_1 = 0$ in Eq. (16) and thus the MT populations are related through:

$$\bar{\mu}_s(x) = \frac{v_g(\bar{M})}{v_s} \bar{\mu}_g(x). \quad (18)$$

To solve for the steady-state MT densities, we plug the relationship in Eq. (18) into Eqs. (14) and find that $\bar{\mu}_g(x)$ satisfies:

$$\frac{\partial}{\partial x} (v_g(\bar{M})\bar{\mu}_g) = \left(\frac{v_g(\bar{M})\lambda_{s \rightarrow g}}{v_s} - \lambda_{g \rightarrow s}(x) \right) \bar{\mu}_g, \quad (19)$$

hence

$$\begin{aligned} \bar{\mu}_g(x) &= c_1 \exp \left(\frac{\lambda_{s \rightarrow g}}{v_s} x - \frac{\int \lambda_{g \rightarrow s}(x') dx'}{v_g(\bar{M})} \right), \\ \bar{\mu}_s(x) &= c_1 \frac{v_g(\bar{M})}{v_s} \exp \left(\frac{\lambda_{s \rightarrow g}}{v_s} x - \frac{\int \lambda_{g \rightarrow s}(x') dx'}{v_g(\bar{M})} \right). \end{aligned} \quad (20)$$

We note that the expressions for $\bar{\mu}_g(x)$ and $\bar{\mu}_s(x)$ in Eqs. (20) depend on the steady-state amount of tubulin in MTs \bar{M} . In turn, \bar{M} also depends on the steady-state solutions for $\bar{\mu}_g(x)$ and $\bar{\mu}_s(x)$:

$$\bar{M} = \int_0^\infty x (\bar{\mu}_g(x) + \bar{\mu}_s(x)) dx. \quad (21)$$

Equation (21) thus consists of an implicit equation for \bar{M} . To solve this, we must find roots \bar{M} that satisfy Eqs. (20) and (21). We use the nonlinear root finder `fzero` in MATLAB and find that a numerical root solution for \bar{M} can be found in the parameter regimes of interest. The steady-state number of MTs and steady-state MT length are then given by:

$$\bar{N} = \int_0^\infty (\bar{\mu}_g(x) + \bar{\mu}_s(x)) dx, \quad (22)$$

$$\bar{L} = \frac{\bar{M}}{\bar{N}}, \quad (23)$$

respectively.

3.2 Steady-state length distributions in different length-regulation regimes

We now derive the solutions for $\bar{\mu}_g(x)$ and $\bar{\mu}_s(x)$ in different regimes of length-dependent catastrophe, as parameterized by γ in Eq. (3). Recall from section 2 that we denote $\gamma_{\text{crit}} = \frac{\lambda^0 - \lambda_{\min}}{L_0}$. For $\gamma < \gamma_{\text{crit}}$, the growth to shrinking switching rate is given by $\lambda_{g \rightarrow s}(x) = \lambda_{g \rightarrow s}^0 + \gamma(x - L_0)$. Using this rate, we solve Eqs. (20) in Appendix A and find that the steady-state MT length distributions are:

$$\begin{aligned} \bar{\mu}_g(x) &= \frac{\nu}{v_g(\bar{M})} \exp \left(-\frac{\gamma(x - L_0)^2}{2v_g(\bar{M})} + \left(\frac{\lambda_{s \rightarrow g}}{v_s} - \frac{\lambda_{g \rightarrow s}^0}{v_g(\bar{M})} \right) x + \frac{\gamma L_0^2}{2v_g(\bar{M})} \right), \\ \bar{\mu}_s(x) &= \frac{\nu}{v_s} \exp \left(-\frac{\gamma(x - L_0)^2}{2v_g(\bar{M})} + \left(\frac{\lambda_{s \rightarrow g}}{v_s} - \frac{\lambda_{g \rightarrow s}^0}{v_g(\bar{M})} \right) x + \frac{\gamma L_0^2}{2v_g(\bar{M})} \right). \end{aligned} \quad (24)$$

Note that this also holds for $\gamma = 0$, corresponding to no length-dependent catastrophe.

For values of $\gamma > \gamma_{\text{crit}}$, it is possible for the rate of growth to shrinking to be $\lambda_{g \rightarrow s}(x) = \lambda_{\min}$. This occurs if the MT length x satisfies

$$x < L_0 + \frac{\lambda_{\min} - \lambda_{g \rightarrow s}^0}{\gamma} = x_{\text{crit}}. \quad (25)$$

For biologically-relevant MT lengths, we require x_{crit} to be nonnegative, which is satisfied for $\gamma > \gamma_{\text{crit}}$. On the other hand, when $x \geq x_{\text{crit}}$, then $\lambda_{g \rightarrow s}(x) = \lambda_{g \rightarrow s}^0 + \gamma(x - L_0)$. Therefore for $\gamma > \gamma_{\text{crit}}$, the steady-state length distributions for growing and shrinking MTs become:

$$\begin{aligned} \bar{\mu}_g(x) &= \begin{cases} \frac{\nu}{v_g(\bar{M})} \exp \left(\frac{\lambda_{s \rightarrow g}}{v_s} x - \frac{\lambda_{\min}}{v_g(\bar{M})} x \right), & \text{if } 0 \leq x < x_{\text{crit}}, \\ \frac{\nu}{v_g(\bar{M})} \exp \left(\frac{\lambda_{s \rightarrow g}}{v_s} x - \frac{\lambda_{\min} x_{\text{crit}} + \lambda_{g \rightarrow s}^0 (x - x_{\text{crit}}) + \frac{\gamma}{2} ((x - L_0)^2 - (x_{\text{crit}} - L_0)^2)}{v_g(\bar{M})} \right), & \text{if } x \geq x_{\text{crit}}, \end{cases} \\ \bar{\mu}_s(x) &= \begin{cases} \frac{\nu}{v_s} \exp \left(\frac{\lambda_{s \rightarrow g}}{v_s} x - \frac{\lambda_{\min}}{v_g(\bar{M})} x \right), & \text{if } 0 \leq x < x_{\text{crit}}, \\ \frac{\nu}{v_s} \exp \left(\frac{\lambda_{s \rightarrow g}}{v_s} x - \frac{\lambda_{\min} x_{\text{crit}} + \lambda_{g \rightarrow s}^0 (x - x_{\text{crit}}) + \frac{\gamma}{2} ((x - L_0)^2 - (x_{\text{crit}} - L_0)^2)}{v_g(\bar{M})} \right), & \text{if } x \geq x_{\text{crit}}, \end{cases} \end{aligned} \quad (26)$$

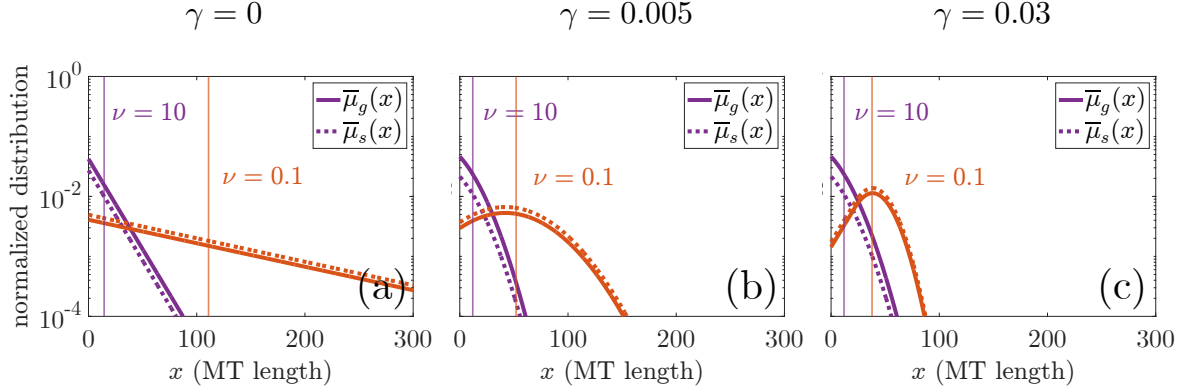


Figure 2: PDE model predictions of steady-state normalized distributions of growing (solid line) and shrinking (dashed line) MTs for $T_{tot} = 1000 \mu\text{m}$ with (a) no length-dependent catastrophe ($\gamma = 0$), (b) low level of length-dependent catastrophe ($\gamma = 0.005$), and (c) high level of length-dependent catastrophe ($\gamma = 0.03$). Red lines correspond to $\nu = 0.1$ and purple lines correspond to $\nu = 10$. Vertical colored lines indicate the steady-state average MT length, $\bar{L} = \bar{M}/\bar{N}$.

respectively. Appendix A provides derivation details for the final solution for the growing and shrinking MT length distributions in Eqs. (24) and (26), including consideration of the boundedness of MT length distributions as imposed in Eq. (17).

4 Results

We study how microtubule nucleation affects steady-state filament lengths and numbers in the PDE model and the stochastic model. We parameterize both model frameworks to achieve the same target steady-state length ($L_* = 35 \mu\text{m}$) with the same baseline total tubulin amount ($T_{tot} = 1000 \mu\text{m}$) [21]. Additional prescribed model parameters can be found in Table 1. For the PDE model, we solve Eqs. (24) or (26), depending on the length-regulating mechanisms considered. Nucleation is implemented by specifying a boundary condition of the PDE system (see Section 3). In the stochastic model, we use the parameterization procedure in [21] and allow new MTs to be nucleated in the stochastic framework as a Poisson process at a fixed rate (see Section 2). The stochastic realizations are run up to 100 hours, and results are collected after one hour of simulation time. We use several values of the nucleation rate and of the length-dependent catastrophe parameter to investigate how these mechanisms impact steady-state MT characteristics.

The steady-state of the PDE model can be calculated analytically, making it tractable to investigate how nucleation, length-dependent catastrophe, and tubulin limitation impact steady-state MT dynamics, length distributions, and overall MT number (Section 4.1). In addition, solving for the steady-state solutions of this continuous model allows us to more easily study the identifiability of model parameters and to assess if different parameter and mechanistic combinations yield a similar average MT length and MT number.

The PDE model is easier to analyze; however, it only describes the dynamics at the plus

end of the MTs. We are therefore interested in understanding the regimes of parameter space where the simplified PDE model captures similar behaviors as several realizations of the more complicated stochastic model (Section 4.2). In particular, we compare the resulting MT length distributions, average MT length, and average MT number from both models.

The stochastic model is more complex due to the many parameters and the computational cost of simulating many model realizations to understand how combinations of mechanisms contribute to emerging properties of MT dynamics (Section 4.3). However, this framework has the advantage that it can capture realistic fluctuations in MT number and tubulin availability. We seek to understand how nucleation impacts the variance in length and number of MTs given stochastic fluctuations in MT growth dynamics and nucleation.

4.1 In the PDE model, small nucleation rates lead to fewer and longer MTs

We aim to understand how nucleation impacts the predicted steady-state MT length distribution in the reduced PDE model in Section 3. Figure 2 shows how the normalized densities of steady-state growing MTs, $\bar{\mu}_g(x)/\bar{N}$, and shrinking MTs, $\bar{\mu}_s(x)/\bar{N}$, are impacted by varying the contribution of the length-dependent catastrophe mechanism and by varying nucleation rates. Figure 2a shows that, without length-dependent catastrophe, the distribution of steady-state MT lengths for both nucleation values is exponential (note the semi-logarithmic scale.)

With length-dependent catastrophe, Figure 2b and 2c show length distributions that are more Gaussian-like, which has also been observed experimentally [41, 42, 43, 44]. All panels in Figure 2 show that, as nucleation increases, the steady state average MT length \bar{L} decreases. In the case where length-dependent catastrophe contributes to MT length regulation, the higher nucleation rate leads to a more exponential-like distribution and shorter MT lengths. Interestingly, for the high nucleation rate examined, the distribution of growing MTs is larger than the distribution of shrinking MTs for all length-dependent catastrophe levels, while the opposite is true for the low nucleation rate. In Eq. (26), we note that the growing and shrinking MT length distributions differ only by the constant $\nu/v_g(\bar{M})$ and ν/v_s , respectively. As nucleation increases, our model predicts that the amount of tubulin in MTs \bar{M} increases. This means that $v_g(\bar{M})$ decreases, and thus explains why the higher nucleation rate results in a larger number of growing MTs at steady-state.

Microtubule nucleation thus clearly affects MT length distributions, but Eqs. (40) suggest that they also impact the average number of MTs at steady state, \bar{N} , and the average length of MTs at steady state, \bar{L} . We also seek to understand how varying the total amount of tubulin available in the cell affects the average number and length of MTs. We therefore investigate how \bar{N} and \bar{L} are affected as T_{tot} and ν are varied. As in [21], we choose a low tubulin level $T_{tot} = 700\mu\text{m}$ and a high tubulin level $T_{tot} = 4000\mu\text{m}$. For the nucleation rate, *in vivo* experiments show that nucleation can be up- or down-regulated by certain signaling pathways in both healthy and injured neurons [36, 33, 6]. We therefore vary the nucleation rate ν across four orders of magnitude ($10^{-2} - 10^1 \text{ min}^{-1}$) to understand the impact of this mechanism for a large range of rates.

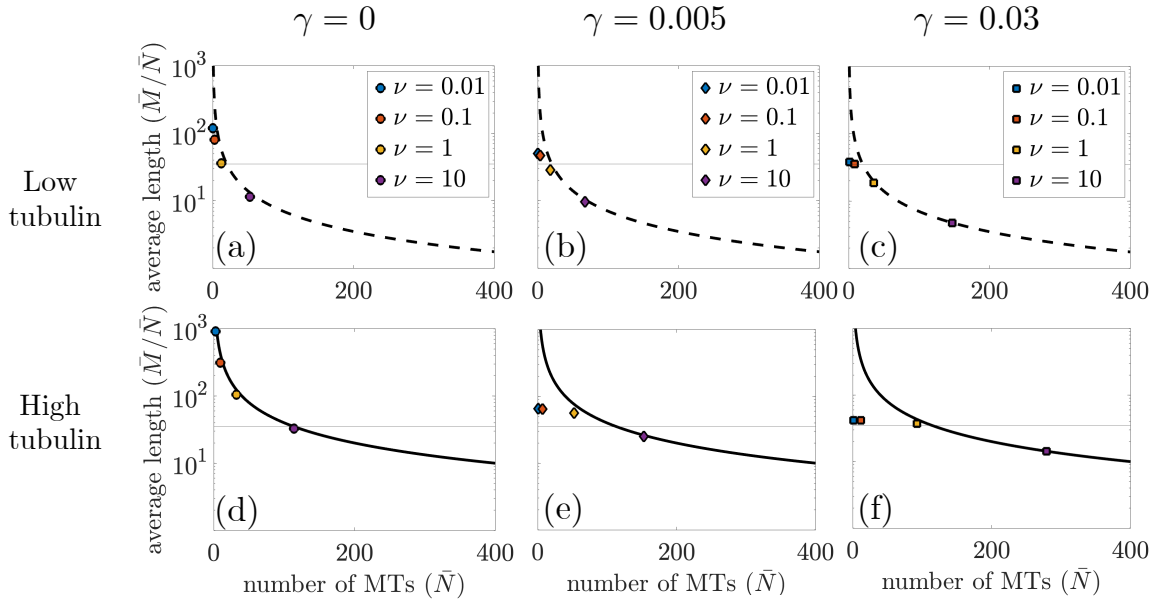


Figure 3: PDE model predictions of average number of MTs, \bar{N} , versus average length of MTs, $\bar{L} = \bar{M}/\bar{N}$, for $T_{\text{tot}} = 700\mu\text{m}$ (top row) and $T_{\text{tot}} = 4000\mu\text{m}$ (bottom row). Results for varying length-dependent catastrophe are shown in the first, second, and third columns, respectively. The circle, diamond, and square marker correspond to $\gamma = 0$, $\gamma = 0.005$, and $\gamma = 0.03$, respectively. The dashed and solid curves represent the tubulin limit found in Eq. (27) for $T_{\text{tot}} = 700\mu\text{m}$ and $T_{\text{tot}} = 4000\mu\text{m}$, respectively, and the horizontal line in each panel represents the target steady-state MT length, L_* .

Figure 3 shows the average number of MTs versus average steady-state MT length for the chosen tubulin levels and nucleation rates. For $T_{tot} = 700\mu\text{m}$, this relationship is shown in panels (a,b,c) and for $T_{tot} = 4000\mu\text{m}$, the results are in panels (d,e,f). Each column in Figure 3 represents this relationship for different levels of length-dependent catastrophe. The horizontal line in each panel indicates the target length $L_* = 35\mu\text{m}$ used to parameterize the models. In particular, the target length impacts the choice of parameters $F_{1/2}, \lambda_{s \rightarrow g}$ in the stochastic and PDE model frameworks. For the steady-state solution of the PDE model, we know that $T_{tot} = \bar{M} + \bar{T}$, where \bar{T} is the steady-state amount of free tubulin. If all tubulin were contained in MTs, then we would expect that:

$$T_{tot} = \bar{M} \times \bar{N}. \quad (27)$$

We visualize the curve $\bar{M} \times \bar{N}$ for $T_{tot} = 700\mu\text{m}$ and $T_{tot} = 4000\mu\text{m}$ with dashed and solid black lines, respectively, in the panels in Figure 3. Note that the closer the markers are to the curve described by Eq. (27), the more tubulin-scarce the system is at steady state.

With no length-dependent catastrophe, Figures 3(a,d) show that for both low and high tubulin amounts, most tubulin is contained in MTs. For low nucleation rates, the average number of MTs is small, while the average MT length is large. As nucleation increases for both tubulin levels, the average MT length decreases and the average MT number increases, while their relationship tightly follows Eq. (27). For each nucleation rate, we see that the average MT length $\bar{L} = \bar{M}/\bar{N}$ is almost an order of magnitude larger for the high tubulin amount compared to the low tubulin amount. Without other length-regulating mechanisms, MT length depends strongly on the total amount of tubulin, as previously seen in [21]. Given the target average MT length $L_* = 35\mu\text{m}$, we find that there exists a nucleation rate ν that achieves L_* for both tubulin levels. This suggests that multiple combinations of mechanisms can result in the same target MT length.

With a low amount of length-dependent catastrophe, $\gamma = 0.005 < \gamma_{\text{crit}}$, Figures 3(b,e) show that average length is more tightly regulated compared to the no length-dependent catastrophe case. This is particularly evident in low nucleation cases, where for both $\nu = 0.01$ and 0.1 , the average lengths for both high and low tubulin do not closely follow the curve from Eq. (27). This suggests that the system in this regime is not tubulin scarce and some amount of tubulin is not contained in MTs. Additionally, the average MT length \bar{L} is similar for low levels of nucleation at both tubulin levels. This suggests that the length-dependent catastrophe mechanism coupled with low nucleation leads to a similar average MT length at a variety of tubulin levels. When $\gamma = 0.03 > \gamma_{\text{crit}}$, indicating high length-dependent catastrophe, Figures 3(c,f) show that the average length is even more tightly regulated than the $\gamma = 0.005$ case, with the average MT length close to L_* for almost all nucleation levels. As with the no length-dependent catastrophe case, MT number increases as nucleation level increases for both levels of length-dependent catastrophe.

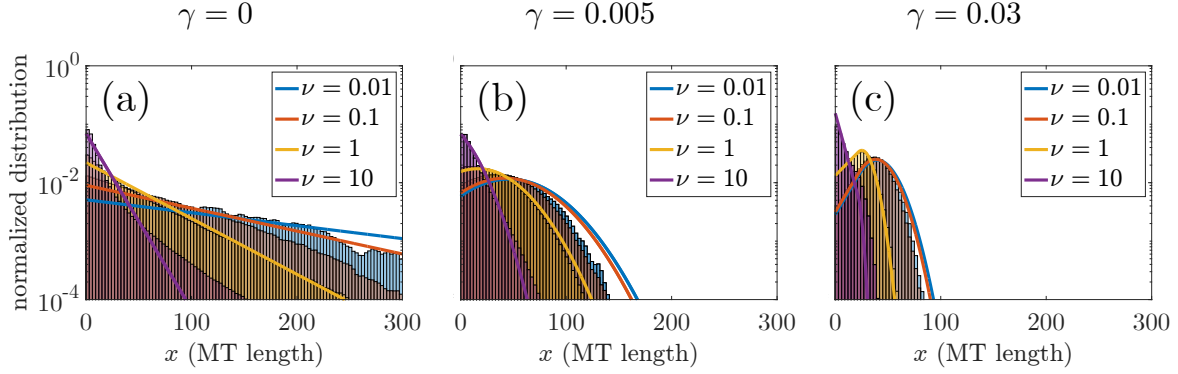


Figure 4: Comparison of steady-state MT length distributions and stochastic MT length distributions for (a) no length-dependent catastrophe, (b) low length-dependent catastrophe, and (c) high length-dependent catastrophe. For all cases, $T_{tot} = 1000\mu\text{m}$. Solid lines show steady state densities of $\bar{\mu}_g(x) + \bar{\mu}_s(x)$ for various levels of nucleation corresponding to Eqs. (24) and (26), depending on the length-dependent catastrophe mechanism. Histograms are generated from 10 realizations of the MT growth dynamic stochastic model, simulated to 100 hours.

4.2 Predictions of MT length distributions from the PDE model are consistent with stochastic model simulations

As discussed in Section 2, the stochastic model of MT length regulation and nucleation allows for dynamics on both MT ends and can be computationally expensive to simulate. Given that the reduced PDE model in Section 4.1 is more analytically tractable, we seek to understand whether the solutions of this reduced model capture the key MT dynamics and steady-state properties reflected by the stochastic model. We are also interested in finding whether there are parameter regimes in which the stochastic model predictions deviate from the continuous model predictions.

In Figure 4, we show MT length distributions for various nucleation rates, and we compare length distributions from ten stochastic realizations with the normalized reduced PDE steady-state MT distributions ($\bar{\mu}(x)/\bar{N}$) for each nucleation rate from either Eq. (24) or Eq. (26). To compare with the steady-state PDE distributions, each realization of the stochastic model is simulated up to 100 hours. The dashed vertical line indicates the target MT length of $35\mu\text{m}$. For each panel, the shape of the MT length distribution for the stochastic simulation agrees well with the distribution from reduced PDE results. The PDE steady-state MT length distribution overestimates the frequency of large MT lengths for small nucleation rates, whereas for large nucleation rates, the PDE results underestimate the frequency of large MTs. As in [21], the length-dependent catastrophe mechanism influences the type of length distribution at steady state. With no length-dependent catastrophe, Figure 4a shows that for each level of nucleation, the MT length distribution is exponential-like. For low and high levels of length-dependent catastrophe in Figures 4(b,c), both the stochastic and reduced PDE results show a Gaussian-like distribution of MT lengths. As nucleation increases in each panel, we see short MT lengths increase in frequency and the

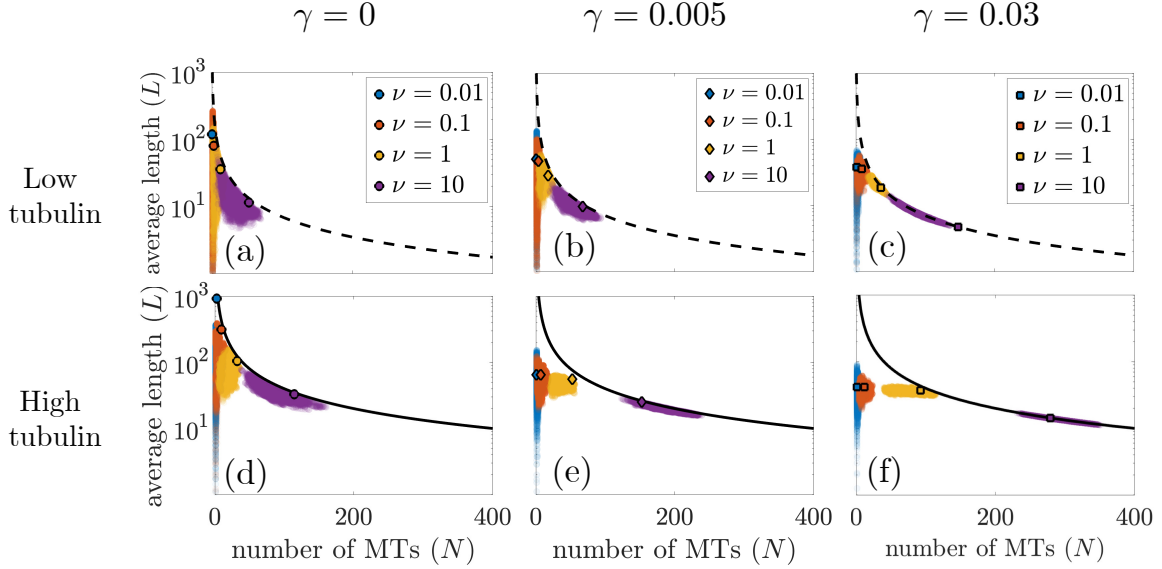


Figure 5: Model predictions of the average number of MTs (\bar{N}) versus the average length of MTs (\bar{L}) from the steady-state PDE solutions (markers outlined in black, same as Fig. 3) and from 10 realizations of the stochastic model (colored point cloud) simulated up to 5 hours. Each point in the point cloud represents a pair consisting of the MT number and the average MT length (N, L) at each time point (second) of the stochastic simulation. Panels (a,d) show results for $\gamma = 0$, panels (b,e) illustrate results for $\gamma = 0.005$, and panels (c,f) represent results when $\gamma = 0.03$. Results for the low tubulin level ($T_{tot} = 700\mu\text{m}$) are given in the top panels (a,b,c) and results for the high tubulin level ($T_{tot} = 4000\mu\text{m}$) are found in the bottom panels (d,e,f). The dashed and solid curves correspond to the tubulin limit found in Eq. (27) for $T_{tot} = 700\mu\text{m}$ and $T_{tot} = 4000\mu\text{m}$, respectively.

average MT length decreases.

4.3 The stochastic model predicts high variance in MT length at low nucleation rate and high variance in MT number at high nucleation rate

Section 4.2 shows that nucleation impacts the MT length distribution in a similar way in both the reduced PDE model framework and the stochastic framework. From Eq. (22), we predict that changes in the MT length distribution also influence the steady-state number of MTs and the average MT length. Therefore, we wish to understand how nucleation affects MT number and average MT length with various length-regulating mechanisms. Again, we can compare the results from the stochastic realizations and the reduced PDE model framework to understand the parameter regimes where stochastic fluctuations most impact MT properties such as MT number and length.

In Figure 5, we study how stochastic fluctuations, tubulin availability, and length-dependent catastrophe impact the relationship between average MT length and MT number

for both the stochastic and reduced PDE model. The markers outlined in black indicate analytical results from the steady-state solution of the reduced PDE model, while the point clouds represent pairs of MT number and length (N, L) for each time step (1 second) of the stochastic realizations. Each realization is simulated up to 5 hours. The top row shows results for low tubulin ($T_{tot} = 700\mu\text{m}$) and the bottom row shows results for high tubulin ($T_{tot} = 4000\mu\text{m}$). In the left column, middle, and right column, we impose the following length-dependent catastrophe parameters for both the PDE and stochastic model: no length-dependent catastrophe ($\gamma = 0$), low length-dependent catastrophe ($\gamma = 0.005$), and high length-dependent catastrophe ($\gamma = 0.03$). As in Figure 3, the dashed and solid black curves correspond to the MT content and number given by the tubulin limit in Eq. (27) for $T_{tot} = 700\mu\text{m}$ and $T_{tot} = 4000\mu\text{m}$, respectively.

First, we compare the results from the reduced PDE model with the stochastic model. For nearly all nucleation rates ν , we find that the steady-state PDE results are within their corresponding stochastic simulation point cloud of MT length and number. Additionally, all markers lie below the black curves corresponding to the tubulin limit. When the markers are close to these curves, the system is in a tubulin-scarce regime and almost all tubulin is contained in MTs. In the low tubulin regime, Figures 5(a,b,c) show that both the stochastic model and the reduced PDE model are fairly close to the tubulin limit. As tubulin increases, the amount of length-dependent catastrophe influences how tubulin-scarce the system is. In Figures 5(e,f), both the stochastic and reduced PDE results for lower levels of nucleation are not at the tubulin limit. This indicates that length-dependent catastrophe plays an important role in increasing the amount of available tubulin in the system. However, when nucleation increases to the highest level we studied ($\nu = 10 \text{ min}^{-1}$), the system is again in the tubulin-scarce regime.

While the reduced PDE model can predict a relationship between average MT length and MT number, results from the stochastic simulations illustrate how fluctuations driven by the dynamic instability of MTs impact this relationship. Across tubulin amounts and length-dependent catastrophe levels, there exists a high variance in MT length and low variance in MT number at low nucleation. As the nucleation rate increases, the variance in MT length decreases while the variance in MT number increases. This is particularly evident in the case of high tubulin and high length-dependent catastrophe in Figure 5f. For low levels of nucleation, the blue point clouds indicate that MT length can vary almost 2 orders of magnitude in the stochastic model, while the MT number stays relatively fixed. When nucleation is high, the variance in the MT length is relatively small while the MT number varies across time and simulations.

5 Conclusion and outlook

In this paper, we propose a stochastic model and a reduced PDE model of MT dynamics and nucleation to understand how MT numbers and length distributions are affected by filament nucleation levels and different length-regulating mechanisms. The stochastic

model is parameterized using the procedure developed in [21]; here, we also incorporate a MT nucleation mechanism using a Poisson process that allows for new MTs to be seeded. This stochastic framework incorporates fluctuations in both tubulin availability and MT nucleation to understand how these mechanisms impact MT properties such as steady-state length distributions and MT numbers. We compare the results from the stochastic model to steady-state results from a simpler PDE model, which allows for MT nucleation and assumes MT growth dynamics on only one end.

With two length-regulating mechanisms (tubulin availability and length-dependent catastrophe), our results show that the MT nucleation rate influences both the steady-state MT length distributions and the number of MTs. In most parameter regimes, the MT length distributions from the reduced PDE model agree well with distributions from the stochastic framework. This is the case despite the fact that the PDE model only accounts for MT plus-end dynamics. The similarities in predictions are especially good in regimes with more length-dependent catastrophe regulation. The relationship between average MT length and average MT number is also similar across the stochastic and reduced PDE model frameworks. In particular, as nucleation increases, the average MT length decreases while the average number of MTs increases.

As reported before [21], these models of MT dynamics exhibit identifiability issues, since multiple combinations of mechanisms can result in the same target MT length. However, the different mechanistic contributions to filament turnover can lead to different distributions in MT length and number. Our stochastic model results illustrate that, as nucleation increases, the MT length distributions become more exponential-like. In addition, the nucleation rate also impacts the amount of variation observed in MT length and number. For low levels of nucleation, we observe high variation in MT length with a regulated low number of MTs. As nucleation increases, the variability in MT length decreases, while the variation in MT number increases.

Here, we are particularly motivated by observations of MT dynamics in experiments of living *Drosophila* neurons, where MT growth dynamics and nucleation have been studied in healthy and injured settings [35, 6, 39, 2]. The results of the models proposed here provide hypotheses that could be validated experimentally. For example, experiments that manipulate tubulin and that up- or down-regulate MT nucleation in neurons have been proposed. The model here has predictive value for such experiments, as it illustrates that different MT length distributions and distinct regulation of MT numbers can be generated in different mechanistic regimes. In particular, the variance in MT length and number depends on the level of MT nucleation in the cell. Given experimental observations, the model could therefore suggest key potential mechanisms of MT dynamics.

More broadly, MTs and other cytoskeleton filaments are polarized structures in healthy neurons (as well as other cells). This polar organization of MT filaments is established and maintained over the course of the lifetime of the organism. Microtubule nucleation is known to be controlled at dendrite branches in neurons and to contribute to the maintenance of polarity. However, it is not known how the stable levels of microtubule dynamics and

organization are maintained over time. Microtubule nucleation is also known to be highly regulated during neural development and altered after neuronal injury. Following axonal injury, MTs are known to display increased nucleation as part of a neuroprotective program [6, 32]. The mathematical models and mechanisms studied here can therefore contribute to our understanding of the mechanisms that control MT polarity and regulation in injury and development.

6 Acknowledgments

This work was supported by NIH grant R01NS121245. ACN was partially supported by NSF grant DMS-2038056. ACN would like to thank UNM's Center for Advanced Research Computing, supported in part by the National Science Foundation, for providing the computing resources and large-scale storage used in this work.

Appendix A Derivation of steady-state microtubule length distributions

Based on Eqs. (20), the steady-state length distributions of growing and shrinking MTs ($\bar{\mu}_g(x)$ and $\bar{\mu}_s(x)$) clearly depend on the length-dependent catastrophe mechanism, which is given by the growth to shrinking rate $\lambda_{g \rightarrow s}(x)$:

$$\lambda_{g \rightarrow s}(x) = \max \left(\lambda_{\min}, \lambda_{g \rightarrow s}^0 + \gamma(x - L_0) \right). \quad (28)$$

We first consider the scenario where $\lambda_{g \rightarrow s}(x)$ is always dependent on length. This means that

$$\lambda_{g \rightarrow s}(x) = \lambda_{g \rightarrow s}^0 + \gamma(x - L_0), \quad \forall x, \quad (29)$$

which in turn means that $\lambda_{\min} < \lambda_{g \rightarrow s}^0 + \gamma(x - L_0)$ for all x . This occurs when $\gamma \leq \frac{\lambda_{g \rightarrow s}^0 - \lambda_{\min}}{L_0} = \gamma_{\text{crit}}$. In this case, using the steady-state solutions in Eq. (20) and the switch rate in Eq. (29) yields the following steady-state length distributions:

$$\begin{aligned} \bar{\mu}_g(x) &= c_1 \exp \left(\frac{\lambda_{s \rightarrow g}}{v_s} x - \frac{\int_0^x \lambda_{g \rightarrow s}^0 + \gamma(x' - L_0) dx'}{v_g(\bar{M})} \right), \\ \bar{\mu}_s(x) &= c_1 \frac{v_g(\bar{M})}{v_s} \exp \left(\frac{\lambda_{s \rightarrow g}}{v_s} x - \frac{\int_0^x \lambda_{g \rightarrow s}^0 + \gamma(x' - L_0) dx'}{v_g(\bar{M})} \right). \end{aligned} \quad (30)$$

Evaluating the integrals, we obtain:

$$\begin{aligned} \bar{\mu}_g(x) &= c_1 \exp \left(\frac{\lambda_{s \rightarrow g}}{v_s} x - \frac{\lambda_{g \rightarrow s}^0 x + \frac{\gamma}{2}(x - L_0)^2 - \frac{\gamma L_0^2}{2}}{v_g(\bar{M})} \right), \\ \bar{\mu}_s(x) &= c_1 \frac{v_g(\bar{M})}{v_s} \exp \left(\frac{\lambda_{s \rightarrow g}}{v_s} x - \frac{\lambda_{g \rightarrow s}^0 x + \frac{\gamma}{2}(x - L_0)^2 - \frac{\gamma L_0^2}{2}}{v_g(\bar{M})} \right). \end{aligned} \quad (31)$$

Using the initial condition $v_g(\bar{M})\bar{\mu}_g(0) = \nu$, we find that the constant is given by $c_1 = \frac{\nu}{v_g(\bar{M})}$.

Therefore, for $\gamma \leq \gamma_{\text{crit}}$, the steady-state growing and shrinking MT length distributions are:

$$\begin{aligned}\bar{\mu}_g(x) &= \frac{\nu}{v_g(\bar{M})} \exp \left(-\frac{\gamma(x-L_0)^2}{2v_g(\bar{M})} + \left(\frac{\lambda_{s \rightarrow g}}{v_s} - \frac{\lambda_{g \rightarrow s}}{v_g(\bar{M})} \right) x + \frac{\gamma L_0^2}{2v_g(\bar{M})} \right), \\ \bar{\mu}_s(x) &= \frac{\nu}{v_s} \exp \left(-\frac{\gamma(x-L_0)^2}{2v_g(\bar{M})} + \left(\frac{\lambda_{s \rightarrow g}}{v_s} - \frac{\lambda_{g \rightarrow s}}{v_g(\bar{M})} \right) x + \frac{\gamma L_0^2}{2v_g(\bar{M})} \right).\end{aligned}\quad (32)$$

Next, we consider the scenario where $\lambda_{\min} > \lambda_{g \rightarrow s}^0 + \gamma(x-L_0)$, which occurs when

$$x < x_{\text{crit}} = L_0 + \frac{\lambda_{\min} - \lambda_{g \rightarrow s}^0}{\gamma}.\quad (33)$$

For this regime to be biologically relevant (positive MT lengths), we must have $x_{\text{crit}} > 0$. This occurs when $\gamma > \gamma_{\text{crit}} = \frac{\lambda_{g \rightarrow s}^0 - \lambda_{\min}}{L_0}$. Therefore, when $\gamma > \gamma_{\text{crit}}$, the growth to shrinking rate is dependent on the MT length in the following way:

$$\lambda_{g \rightarrow s}(x) = \begin{cases} \lambda_{\min} & \text{if } 0 \leq x < x_{\text{crit}}, \\ \lambda_{g \rightarrow s}^0 + \gamma(x-L_0) & \text{if } x \geq x_{\text{crit}}. \end{cases}\quad (34)$$

The steady-state growing and shrinking MT length distributions in this setting are:

$$\begin{aligned}\bar{\mu}_g(x) &= \begin{cases} c_1 \exp \left(\frac{\lambda_{s \rightarrow g}}{v_s} x - \frac{\int_0^x \lambda_{\min} dx'}{v_g(\bar{M})} \right), & \text{if } 0 \leq x < x_{\text{crit}}, \\ c_2 \exp \left(\frac{\lambda_{s \rightarrow g}}{v_s} x - \frac{\int_0^{x_{\text{crit}}} \lambda_{\min} dx' + \int_{x_{\text{crit}}}^x \lambda_{g \rightarrow s}^0 + \gamma(x'-L_0) dx'}{v_g(\bar{M})} \right), & \text{if } x \geq x_{\text{crit}}. \end{cases} \\ \bar{\mu}_s(x) &= \begin{cases} c_1 \frac{v_g(\bar{M})}{v_s} \exp \left(\frac{\lambda_{s \rightarrow g}}{v_s} x - \frac{\int_0^x \lambda_{\min} dx'}{v_g(\bar{M})} \right), & \text{if } 0 \leq x < x_{\text{crit}}, \\ c_2 \frac{v_g(\bar{M})}{v_s} \exp \left(\frac{\lambda_{s \rightarrow g}}{v_s} x - \frac{\int_0^{x_{\text{crit}}} \lambda_{\min} dx' + \int_{x_{\text{crit}}}^x \lambda_{g \rightarrow s}^0 + \gamma(x'-L_0) dx'}{v_g(\bar{M})} \right), & \text{if } x \geq x_{\text{crit}}. \end{cases}\end{aligned}\quad (35)$$

Evaluating the integrals yields

$$\begin{aligned}\bar{\mu}_g(x) &= \begin{cases} c_1 \exp \left(\frac{\lambda_{s \rightarrow g}}{v_s} x - \frac{\lambda_{\min}}{v_g(\bar{M})} x \right), & \text{if } 0 \leq x < x_{\text{crit}}, \\ c_2 \exp \left(\frac{\lambda_{s \rightarrow g}}{v_s} x - \frac{\lambda_{\min} x_{\text{crit}} + \lambda_{g \rightarrow s}^0 (x - x_{\text{crit}}) + \frac{\gamma}{2} ((x-L_0)^2 - (x_{\text{crit}}-L_0)^2)}{v_g(\bar{M})} \right), & \text{if } x \geq x_{\text{crit}}. \end{cases} \\ \bar{\mu}_s(x) &= \begin{cases} c_1 \frac{v_g(\bar{M})}{v_s} \exp \left(\frac{\lambda_{s \rightarrow g}}{v_s} x - \frac{\lambda_{\min}}{v_g(\bar{M})} x \right), & \text{if } 0 \leq x < x_{\text{crit}}, \\ c_2 \frac{v_g(\bar{M})}{v_s} \exp \left(\frac{\lambda_{s \rightarrow g}}{v_s} x - \frac{\lambda_{\min} x_{\text{crit}} + \lambda_{g \rightarrow s}^0 (x - x_{\text{crit}}) + \frac{\gamma}{2} ((x-L_0)^2 - (x_{\text{crit}}-L_0)^2)}{v_g(\bar{M})} \right), & \text{if } x \geq x_{\text{crit}}. \end{cases}\end{aligned}\quad (36)$$

Using initial condition $v_g(\bar{M})\bar{\mu}_g(0) = \nu$ and Eqs. (36), we again obtain:

$$c_1 = \frac{\nu}{v_g(\bar{M})}.\quad (37)$$

We require continuity through $\lim_{x \rightarrow x_{\text{crit}}^-} \bar{\mu}_g(x) = \lim_{x \rightarrow x_{\text{crit}}^+} \bar{\mu}_g(x)$, which implies that

$$\frac{\nu}{v_g(\bar{M})} \exp \left(\left(\frac{\lambda_{s \rightarrow g}}{v_s} - \frac{\lambda_{\min}}{v_g(\bar{M})} \right) x_{\text{crit}} \right) = c_2 \exp \left(\frac{\lambda_{s \rightarrow g}}{v_s} x_{\text{crit}} - \frac{\lambda_{\min} x_{\text{crit}}}{v_g(\bar{M})} \right), \quad (38)$$

so that

$$c_2 = \frac{\nu}{v_g(\bar{M})} = c_1. \quad (39)$$

Therefore, the steady-state solutions in parameter setting are:

$$\begin{aligned} \bar{\mu}_g(x) &= \begin{cases} \frac{\nu}{v_g(\bar{M})} \exp \left(\frac{\lambda_{s \rightarrow g}}{v_s} x - \frac{\lambda_{\min}}{v_g(\bar{M})} x \right), & \text{if } 0 \leq x < x_{\text{crit}}, \\ \frac{\nu}{v_g(\bar{M})} \exp \left(\frac{\lambda_{s \rightarrow g}}{v_s} x - \frac{\lambda_{\min} x_{\text{crit}} + \lambda_{g \rightarrow s}^0 (x - x_{\text{crit}}) + \frac{\gamma}{2} ((x - L_0)^2 - (x_{\text{crit}} - L_0)^2)}{v_g(\bar{M})} \right), & \text{if } x \geq x_{\text{crit}}. \end{cases} \\ \bar{\mu}_s(x) &= \begin{cases} \frac{\nu}{v_s} \exp \left(\frac{\lambda_{s \rightarrow g}}{v_s} x - \frac{\lambda_{\min}}{v_g(\bar{M})} x \right), & \text{if } 0 \leq x < x_{\text{crit}}, \\ \frac{\nu}{v_s} \exp \left(\frac{\lambda_{s \rightarrow g}}{v_s} x - \frac{\lambda_{\min} x_{\text{crit}} + \lambda_{g \rightarrow s}^0 (x - x_{\text{crit}}) + \frac{\gamma}{2} ((x - L_0)^2 - (x_{\text{crit}} - L_0)^2)}{v_g(\bar{M})} \right), & \text{if } x \geq x_{\text{crit}}. \end{cases} \end{aligned} \quad (40)$$

Note that the solutions in Eqs. (32) and (40) contain exponential functions of the form e^{ax^2+bx+c} . Since we seek bounded steady-state MT lengths, we note that:

$$\lim_{x \rightarrow \infty} e^{ax^2+bx+c} = \begin{cases} \infty, & \text{if } a > 0 \\ 0, & \text{if } a < 0. \end{cases} \quad (41)$$

In our case, $a = -\frac{\gamma}{2v_g(\bar{M})}$, so as long as $\gamma > 0$, $\lim_{x \rightarrow \infty} \bar{\mu}_g(x) = \lim_{x \rightarrow \infty} \bar{\mu}_s(x) = 0$ and thus MT lengths remain bounded.

In the case where $\gamma = 0$, the model does not include a length-dependent catastrophe mechanism. In this case, $\lambda_{g \rightarrow s}(x) = \lambda_{g \rightarrow s}^0 + \gamma(x - L_0) = \lambda_{g \rightarrow s}^0$ and Eqs. (20) become:

$$\begin{aligned} \bar{\mu}_g(x) &= \frac{\nu}{v_g(\bar{M})} \exp \left(\left(\frac{\lambda_{s \rightarrow g}}{v_s} - \frac{\lambda_{g \rightarrow s}^0}{v_g(\bar{M})} \right) x \right), \\ \bar{\mu}_s(x) &= \frac{\nu}{v_s} \exp \left(\left(\frac{\lambda_{s \rightarrow g}}{v_s} - \frac{\lambda_{g \rightarrow s}^0}{v_g(\bar{M})} \right) x \right). \end{aligned} \quad (42)$$

We are again interested in the behavior of these distributions in the limit that $x \rightarrow \infty$. To achieve bounded MT length distributions, we must have that:

$$v_g(\bar{M}) \lambda_{s \rightarrow g} < \lambda_{g \rightarrow s}^0 v_s. \quad (43)$$

In Table 1, we note that $\lambda_{g \rightarrow s}^0 = 0.5 \text{ min}^{-1}$ and $v_s = 6 \mu\text{m}/\text{min}$ for our fruit fly neuron system. Using the parameterization procedure outlined in [21] with $L_* = 35 \mu\text{m}$ and no length-dependent catastrophe, we find that $\lambda_{s \rightarrow g} = 0.3592 \text{ min}^{-1}$. Given these parameter values, and to achieve bounded MT lengths, we must have that $v_g(\bar{M}) < 8.35 \mu\text{m}/\text{min}$, which we achieve through the restriction of growth speed $v_g(\bar{M})$ in Eq. (6) due to tubulin constraints. In conclusion, the upper bound on $v_g(\bar{M})$ and the form of $v_g(\bar{M})$ guarantee that we obtain bounded model MT lengths in this application, even for the case that does not incorporate a length-dependent catastrophe mechanism.

References

- [1] Michael T Kelliher, Harriet AJ Saunders, and Jill Wildonger. Microtubule control of functional architecture in neurons. *Current opinion in neurobiology*, 57:39–45, 2019.
- [2] Melissa M. Rolls, Pankajam Thyagarajan, and Chengye Feng. Microtubule dynamics in healthy and injured neurons. *Developmental Neurobiology*, 81:321–332, 4 2021.
- [3] Tim Mitchison and Marc Kirschner. Dynamic instability of microtubule growth. *nature*, 312(5991):237–242, 1984.
- [4] Neus Teixidó-Travesa, Joan Roig, and Jens Lüders. The where, when and how of microtubule nucleation—one ring to rule them all. *Journal of cell science*, 125(19):4445–4456, 2012.
- [5] Arshad Desai and Timothy J Mitchison. Microtubule polymerization dynamics. *Annual review of cell and developmental biology*, 13(1):83–117, 1997.
- [6] Alexis T Weiner, Pankajam Thyagarajan, Yitao Shen, and Melissa M Rolls. To nucleate or not, that is the question in neurons. *Neuroscience letters*, 751:135806, 2021.
- [7] Jens Lüders. Nucleating microtubules in neurons: Challenges and solutions. *Developmental neurobiology*, 81(3):273–283, 2021.
- [8] Stanislav Vinopal and Frank Bradke. Centrosomal and acentrosomal microtubule nucleation during neuronal development. *Current Opinion in Neurobiology*, 92:103016, 2025.
- [9] Manoj Gopalakrishnan and Bindu S Govindan. A first-passage-time theory for search and capture of chromosomes by microtubules in mitosis. *Bulletin of mathematical biology*, 73:2483–2506, 2011.
- [10] Bela M Mulder. Microtubules interacting with a boundary: Mean length and mean first-passage times. *Physical Review E—Statistical, Nonlinear, and Soft Matter Physics*, 86(1):011902, 2012.
- [11] Terrell L Hill. Introductory analysis of the gtp-cap phase-change kinetics at the end of a microtubule (aggregation/polymer in solution/polymer on site/steady-state distribution). *Proceedings of the National Academy of Sciences*, 81:6728–6732, 1984.
- [12] Robert J Rubin. Mean lifetime of microtubules attached to nucleating sites. *Proceedings of the National Academy of Sciences*, 85(2):446–448, 1988.
- [13] Marileen Dogterom and Stanislas Leibler. Physical aspects of the growth and regulation of microtubule structures microtubules (mts) are long, rigid polymers made of tubulin—a globular protein found in eukaryotic cells [1]. *Physical Review Letters*, 70:1347–1350, 1993.

- [14] Björn Zelinski, Nina Müller, and Jan Kierfeld. Dynamics and length distribution of microtubules under force and confinement. *Physical Review E—Statistical, Nonlinear, and Soft Matter Physics*, 86(4):041918, 2012.
- [15] V Jemseena and Manoj Gopalakrishnan. Effects of aging in catastrophe on the steady state and dynamics of a microtubule population. *Physical Review E*, 91(5):052704, 2015.
- [16] M Dogterom, A C Maggs, and S Leibler. Diffusion and formation of microtubule asters: physical processes versus biochemical regulation. *Proceedings of the National Academy of Sciences*, 92:6683–6688, 1995.
- [17] P. A. Deymier, Y. Yang, and J. Hoying. Effect of tubulin diffusion on polymerization of microtubules. *Physical Review E - Statistical, Nonlinear, and Soft Matter Physics*, 72, 8 2005.
- [18] Gennady Margolin, Ivan V. Gregoret, Holly V. Goodson, and Mark S. Alber. Analysis of a mesoscopic stochastic model of microtubule dynamic instability. *Physical Review E - Statistical, Nonlinear, and Soft Matter Physics*, 74, 2006.
- [19] Peter Hinow, Vahid Rezania, and Jack A Tuszyński. Continuous model for microtubule dynamics with catastrophe, rescue, and nucleation processes. *Physical Review E*, 80(3):031904, 2009.
- [20] Gavin A. Buxton, Sandra L. Siedlak, George Perry, and Mark A. Smith. Mathematical modeling of microtubule dynamics: Insights into physiology and disease. *Progress in Neurobiology*, 92:478–483, 12 2010.
- [21] Anna C Nelson, Melissa M Rolls, Maria-Veronica Ciocanel, and Scott A McKinley. Minimal mechanisms of microtubule length regulation in living cells. *Bulletin of Mathematical Biology*, 86(5):58, 2024.
- [22] H Bolterauer, H-J Limbach, and JA Tuszyński. Models of assembly and disassembly of individual microtubules: stochastic and averaged equations. *Journal of biological physics*, 25:1–22, 1999.
- [23] Bindu S Govindan, Manoj Gopalakrishnan, and Debashish Chowdhury. Length control of microtubules by depolymerizing motor proteins. *Europhysics Letters*, 83(4):40006, 2008.
- [24] I. Mazilu, G. Zamora, and J. Gonzalez. A stochastic model for microtubule length dynamics. *Physica A: Statistical Mechanics and its Applications*, 389:419–427, 2 2010.
- [25] Christian Tischer, Pieter Rein Ten Wolde, and Marileen Dogterom. Providing positional information with active transport on dynamic microtubules. *Biophysical journal*, 99(3):726–735, 2010.

- [26] Hui-Shun Kuan and MD Betterton. Biophysics of filament length regulation by molecular motors. *Physical biology*, 10(3):036004, 2013.
- [27] Matthias Rank, Aniruddha Mitra, Louis Reese, Stefan Diez, and Erwin Frey. Limited resources induce bistability in microtubule length regulation. *Physical Review Letters*, 120, 4 2018.
- [28] Stéphane Honoré, Florence Hubert, Magali Tournus, and Diana White. A growth-fragmentation approach for modeling microtubule dynamic instability. *Bulletin of Mathematical Biology*, 81:722–758, 2019.
- [29] Ivan V Gregoret, Gennady Margolin, Mark S Alber, and Holly V Goodson. Insights into cytoskeletal behavior from computational modeling of dynamic microtubules in a cell-like environment. *Journal of cell science*, 119(22):4781–4788, 2006.
- [30] Kunalika Jain, Jashaswi Basu, Megha Roy, Jyoti Yadav, Shivprasad Patil, and Chaitanya A Athale. Polymerization kinetics of tubulin from mung seedlings modeled as a competition between nucleation and gtp-hydrolysis rates. *Cytoskeleton*, 78(9):436–447, 2021.
- [31] Juan Tao, Chengye Feng, and Melissa M. Rolls. The microtubule-severing protein fidgetin acts after dendrite injury to promote their degeneration. *Journal of Cell Science*, 129:3274–3281, 2016.
- [32] Li Chen, Michelle C Stone, Juan Tao, and Melissa M Rolls. Axon injury and stress trigger a microtubule-based neuroprotective pathway. *Proceedings of the National Academy of Sciences*, 109(29):11842–11847, 2012.
- [33] James I Hertzler, Samantha I Simonovitch, Richard M Albertson, Alexis T Weiner, Derek MR Nye, and Melissa M Rolls. Kinetochore proteins suppress neuronal microtubule dynamics and promote dendrite regeneration. *Molecular biology of the cell*, 31(18):2125–2138, 2020.
- [34] Michelle C Stone, Michelle M Nguyen, Juan Tao, Dana L Allender, and Melissa M Rolls. Global up-regulation of microtubule dynamics and polarity reversal during regeneration of an axon from a dendrite. *Molecular Biology of the Cell*, 21:767–777, 2010.
- [35] Michelle M Nguyen, Christie J McCracken, ES Milner, Daniel J Goetschius, Alexis T Weiner, Melissa K Long, Nick L Michael, Sean Munro, and Melissa M Rolls. γ -tubulin controls neuronal microtubule polarity independently of golgi outposts. *Molecular biology of the cell*, 25(13):2039–2050, 2014.
- [36] Alexis T Weiner, Dylan Y Seebold, Pedro Torres-Gutierrez, Christin Folker, Rachel D Swope, Gregory O Kothe, Jessica G Stoltz, Madeleine K Zalenski, Christopher Kozlowski, Dylan J Barbera, et al. Endosomal wnt signaling proteins control microtubule nucleation in dendrites. *PLoS biology*, 18(3):e3000647, 2020.

- [37] Tatjana Kleele, Petar Marinković, Philip R Williams, Sina Stern, Emily E Weigand, Peter Engerer, Ronald Naumann, Jana Hartmann, Rosa M Karl, Frank Bradke, et al. An assay to image neuronal microtubule dynamics in mice. *Nature communications*, 5(1):4827, 2014.
- [38] Xiaoyi Qu, Atul Kumar, Heike Blockus, Clarissa Waites, and Francesca Bartolini. Activity-dependent nucleation of dynamic microtubules at presynaptic boutons controls neurotransmission. *Current biology*, 29(24):4231–4240, 2019.
- [39] Chengye Feng, Pankajam Thyagarajan, Matthew Shorey, Dylan Y. Seebold, Alexis T. Weiner, Richard M. Albertson, Kavitha S. Rao, Alvaro Sagasti, Daniel J. Goetschius, and Melissa M. Rolls. Patronin-mediated minus end growth is required for dendritic microtubule polarity. *Journal of Cell Biology*, 218:2309–2328, 2019.
- [40] Paul C Bressloff and Hyunjoong Kim. Search-and-capture model of cytoneme-mediated morphogen gradient formation. *Physical Review E*, 99(5):052401, 2019.
- [41] Melissa K Gardner, Marija Zanic, Christopher Gell, Volker Bormuth, and Jonathon Howard. Depolymerizing kinesins kip3 and mcak shape cellular microtubule architecture by differential control of catastrophe. *Cell*, 147(5):1092–1103, 2011.
- [42] Melissa K Gardner, Marija Zanic, and Jonathon Howard. Microtubule catastrophe and rescue. *Current opinion in cell biology*, 25(1):14–22, 2013.
- [43] Lynne U Cassimeris, Patricia Wadsworth, and ED Salmon. Dynamics of microtubule depolymerization in monocytes. *The Journal of cell biology*, 102(6):2023–2032, 1986.
- [44] Eric Schulze and Marc Kirschner. Microtubule dynamics in interphase cells. *The Journal of cell biology*, 102(3):1020–1031, 1986.